Neuron, Volume 61

Supplemental Data

Local origin of field potentials in visual cortex

Steffen Katzner, Ian Nauhaus, Andrea Benucci, Vincent Bonin, Dario L. Ringach, and Matteo Carandini

Supplemental Text

Experimental procedures

Animal preparation

Procedures were approved by the Animal Care and Use Committee of the Smith-Kettlewell Eye Research Institute. Adult cats were initially anesthetized with Ketamine (22 mg/kg) and Xylazine (1.1 mg/kg). Following venous cannulation and tracheotomy, anesthesia was maintained with Fentanyl (typically 10 µg/kg/hr, i.v.), supplemented by inhalation of N_2O mixed with O_2 (typically in a ratio of 70:30), and, as needed, with Sodium Pentothal (up to 2 mg/kg/hr, i.v.). A craniotomy was performed over area V1. The pupils were dilated with atropine. Nictitating membranes were retracted with phenylephrine, and the eyes were protected with gas-permeable contact lenses. Muscle relaxation was induced with Pancuronium Bromide (0.15 mg/kg/hr, i.v.). The animals were artificially respirated and received an antibiotic (Cephazolin, 20 mg/kg, i.m., twice a day) an anti-cholinergic agent (Atropine sulfate, 0.05 mg/kg, i.m., daily), and an anti-inflammatory steroid (Dexamethasone, 0.4 mg/kg, i.m., daily). Fluid balance was maintained by intravenous infusion. Body temperature was maintained near 37°C. Depth of anesthesia was assessed from the EEG, the heart rate, and the level of expired CO_2 concentration. To confirm the validity of these assessments we occasionally interrupted the administration of muscle relaxants to test the depth of anesthesia, and never found it lacking.

Maps of orientation preference were obtained as described elsewhere (Benucci et al., 2007). Briefly, we stained the cortex with the voltage-sensitive dye (VSD) RH-1692, and imaged its fluorescence with a CMOS digital camera (1M60 DALSA, Ontario, Canada) as part of the Imager 3001 setup (Optical Imaging Inc, Rehovot, Israel). Images were acquired at 110 Hz with a resolution of 56 μm per pixel. Additional spatial filtering was performed off-line (band-pass, 0.2-2.2

cycles/mm). Stimulus onset and frame acquisition were synchronized with the respirator. Illumination was provided by a halogen light and delivered through optic fibers. The excitation filter was band-pass (630 $\pm$ 10 nm), and the emission filter was high-pass (> 665 nm).

Having obtained maps of orientation preference, we implanted a 10x10 microelectrode array with an electrode length of 1.5 mm and a grid spacing of 400 μm (Cyberkinetics Neurotechnology Systems, Foxborough, Massachusetts, USA). Across the array, the impedance varied between 0.1 and 0.8 MΩ. Methods for these recordings are provided elsewhere (Nauhaus and Ringach, 2007). Briefly, the array was inserted in the cortex at high speed (~8 m/s) with a pneumatic device. The array and the surrounding tissue were covered with 2% agar to improve stability. Signals were digitized at 30 kHz. LFPs were extracted through bandpass filtering (0.3 Hz-500 Hz) and sampled at 2 kHz. Spikes were extracted by bandpass filtering between 250 Hz and 7.5 kHz. Signals that crossed an appropriate threshold were saved to disk and defined as multi-unit activity (MUA).

Visual stimulation

Stimuli were generated with the Psychophysics toolbox and displayed 57 cm away on a CRT monitor (Sony Trinitron 500PS, mean luminance 32 cd/m^2, refresh rate 120 Hz). We used large (30 deg) sine-wave gratings at 50% contrast. The spatial frequency was optimized for each experiment (0.1-0.4 cycles/deg). Orientation noise stimuli consisted of a sequence of gratings flashed for 32 ms each, randomly varying in orientation (6-12 values) and spatial phase (4 values). Each sequence typically lasted 6-12 s. In cats 1 and 3 we randomly interspersed blank frames between the gratings. Standing gratings contrast-reversed at 4 Hz, lasted 4 s, and had one of 12 orientations and one of 4 spatial phases. Stimuli were repeated in 5-10 trials and stimulus order in each trial was randomized.

References

Benucci, A., Frazor, R.A., and Carandini, M. (2007). Standing Waves and Traveling Waves Distinguish Two Circuits in Visual Cortex. Neuron *55*, 103-117.

Nauhaus, I., Benucci, A., Carandini, M., and Ringach, D.L. (2008). Neuronal Selectivity and Local Map Structure in Visual Cortex. Neuron *57*, 673-679.

Nauhaus, I., and Ringach, D.L. (2007). Precise Alignment of Micromachined Electrode Arrays With V1 Functional Maps. J. Neurophysiol. *97*, 3781--3789.

Supplementary Figure 1. Relation between local map structure and predictability of LFP tuning curves. For each electrode, we quantified the local structure of the orientation preference map by computing an homogeneity index (Nauhaus et al., 2008). This index ranges from 0 to 1. High values represent regions with homogeneous orientation preference (such as iso-orientation domains), low values represent regions with diverse orientation preferences (such as near pinwheel centers). The model performance is quantified by computing the percentage of variance in the measured LFP tuning curves (black dots in Figure 2**F**) that is explained by the spatial integration model based on the orientation maps (red traces in Figure 2**F**). In regions with homogeneous orientation preference, the model yields a better description of measured LFP tuning curves ($r = 0.38$, $p = 0.008$, robust regression).

Supplementary Figure 2. Time course of induced gamma-band activity. (**A**) Spectrogram of induced activity measured at the orientation orthogonal to the preferred orientation for the recording site shown in Figure 1**A-E**. To compute the spectrogram, a sliding hamming window was used on short intervals of the LFP response (65 ms), during which the presentation of a grating was followed by the presentation of a blank screen. From each interval, the evoked component had been removed before by subtracting the mean across intervals. White lines indicate the gamma band (25-90 Hz). (**B**) Same, for the preferred orientation. (**C**) Separability analysis of the induced gamma band activity. The orientation time image (**C**) was obtained by computing the average amplitude within the gamma frequency band. The best separable approximation to this response was obtained with Singular Value Decomposition. The model captures the data very well (middle panel), which is also evidenced by the absence of any structure in the residual image (right panel). The high degree of separability indicates that the induced gamma band activity has an orientation tuning that is constant over time.

Supplementary Figure 3. LFP selectivity and integration area estimated without subtracting the mean response across recording sites. This figure reports the results of performing the same analysis as in Figures 1-2 without removing the mean across sites. (**A**) Selectivity of the single recording site shown in Figure 1**A-E**. (**B**) Selectivity across the entire electrode array. (**C**) Relation between orientation preference of LFPs and simultaneously recorded multi-unit spike activity. (**D**) Relation between predicted and measured LFP responses, across all orientations and recording sites, as a function of the radius of integration. The correlation peaks at a radius of $\sigma = 100$ μm ($r = 0.69$, $p<0.0001$). (**E**) Relation

between orientation preference of predicted and measured LFPs at the optimal radius of integration (σ = 100 μm). Conventions as in Figures 1-2.

Supplementary Figure 1

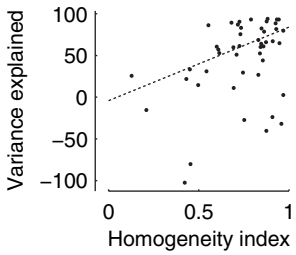

Supplementary Figure 2

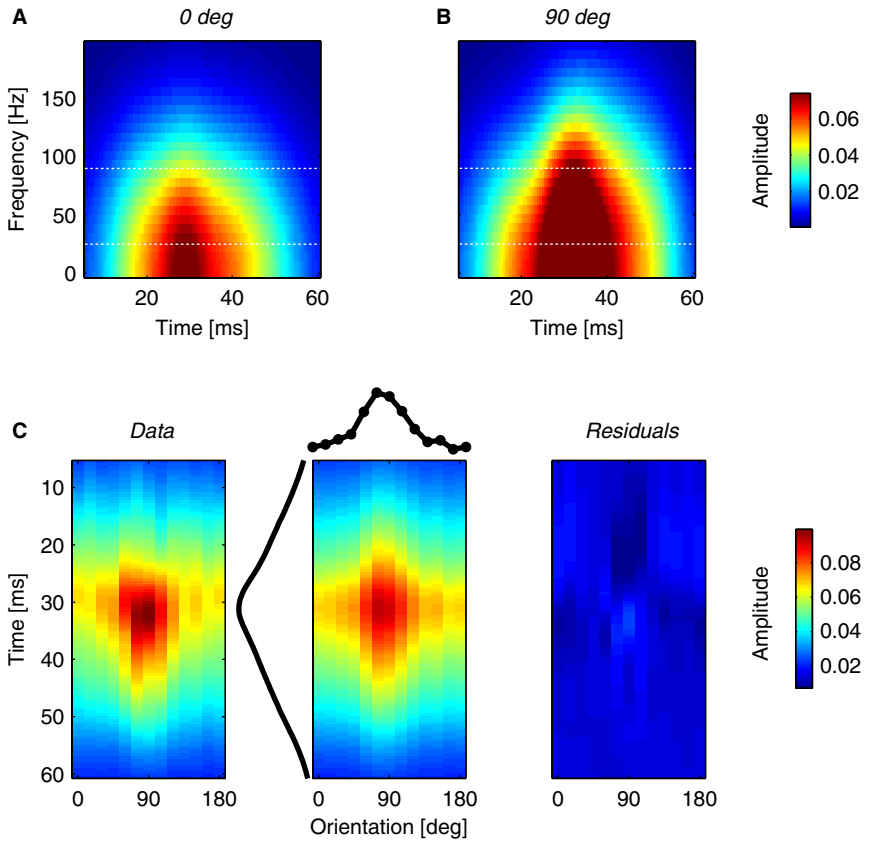

Supplementary Figure 3